HHS Public Access

Author manuscript

*FASEB J.* Author manuscript; available in PMC 2023 December 01.

Published in final edited form as:

*FASEB J.* 2022 December ; 36(12): e22666. doi:10.1096/fj.202201583R.

# Targeted ablation of Fn14 receptor improves exercise capacity and inhibits neurogenic muscle atrophy

**Meiricris Tomaz da Silva**[1], **Aniket S. Joshi**[1], **Tatiana E. Koike**[1], **Anirban Roy**[1], **Kavya Mathukumalli**[1], **Danesh H. Sopariwala**[2], **Vihang A. Narkar**[2], **Ashok Kumar**[1,*]

[1]Department of Pharmacological and Pharmaceutical Sciences, University of Houston College of Pharmacy, Houston, TX 77204, USA

[2]Brown Foundation Institute of Molecular Medicine, McGovern Medical School at The University of Texas Health Science Center (UTHealth), Houston, TX, USA

## Abstract

Skeletal muscle atrophy is a prevalent complication in multiple chronic diseases and disuse conditions. Fibroblast growth factor-inducible 14 (Fn14) is a member of the TNF receptor superfamily and a bona fide receptor of the TWEAK cytokine. Accumulating evidence suggests that Fn14 levels are increased in catabolic conditions as well as during exercise. However, the role of Fn14 in the regulation of skeletal muscle mass and function remains poorly understood. In this study, through the generation of novel skeletal muscle-specific Fn14-knockout mice, we have investigated the muscle role of Fn14 in the regulation of exercise capacity and denervation-induced muscle atrophy. Our results demonstrate that there was no difference in skeletal muscle mass between control and muscle-specific Fn14-knockout mice. Nevertheless, the deletion of Fn14 in skeletal muscle significantly improved exercise capacity and resistance to fatigue. This effect of Fn14 deletion is associated with an increased proportion of oxidative myofibers and higher capillaries number per myofiber in skeletal muscle. Furthermore, our results demonstrate that targeted deletion of Fn14 inhibits denervation-induced muscle atrophy in adult mice. Deletion of Fn14 reduced the expression of components of the ubiquitin-proteasome system and non-canonical NF-kappa B signaling in denervated skeletal muscle, as well as increased the phosphorylation of Akt kinase and FoxO3a transcription factor. Collectively, our results demonstrate that targeted inhibition of Fn14 improves exercise tolerance and inhibits denervation-induced muscle atrophy in adult mice.

[*]**Corresponding author:** Ashok Kumar, Ph.D., Department of Pharmacological and Pharmaceutical Sciences, Health Building 2, Room 5012, College of Pharmacy, University of Houston, 4349 Martin Luther King Boulevard, Houston, TX 77204-1217, Phone: 713-743-3376, akumar43@Central.UH.EDU.

**AUTHOR CONTRIBUTIONS:** Ashok Kumar and Vihang Narkar conceived and designed the research; Meiricris Tomaz da Silva, Aniket Joshi, Tatiana Koike, Anirban Roy, Kavya Mathukumalli, and Danesh H. Sopariwala performed the experiments. Meiricris Tomaz da Silva, Vihang Narkar, and Ashok Kumar interrupted the results of the experiments. Meiricris Tomaz da Silva and Anirban Roy prepared the figures. Meiricris Tomaz da Silva and Ashok Kumar wrote the initial draft of the manuscript. All authors edited and approved the final version of the manuscript.

**CONFLICT OF INTEREST STATEMENT:** The authors have stated explicitly that there are no conflicts of interest in connection with this article.

**Keywords**

Skeletal muscle atrophy; Cytokine signaling; NF-kappa B; FOXO; Angiogenesis

## INTRODUCTION

Skeletal muscle is the most abundant and highly plastic tissue of the human body that functions as a crucial regulator of whole-body metabolism and exercise capacity. Maintenance of healthy muscle mass reduces the morbidity and mortality associated with various chronic diseases and disuse conditions (1, 2). While nutritional uptake and resistance exercise improve skeletal muscle mass and function, various catabolic stimuli including functional denervation lead to the loss of skeletal muscle mass, also known as atrophy (3, 4). At the biochemical level, muscle atrophy involves disruption in proteostasis, especially due to enhanced activation of proteolytic systems, such as the ubiquitin-proteasome system (UPS) and autophagy-lysosomal system. (2, 5, 6). Furthermore, it is now increasingly clear that multiple signaling pathways, such as nuclear factor-κB (NF-κB), p38 MAPK, TGFβ/Myostatin/Activin, Bone morphogenetic proteins, and Akt/FOXO regulate protein content and skeletal muscle mass and function in various physiological and pathophysiological conditions (2, 3, 5, 7).

Fibroblast growth factor-inducible 14 (Fn14, gene name: *TNFRSF12A*) is a member of the TNF receptor superfamily that has been identified as a bona fide receptor for TWEAK cytokine (8–11). The ligand TWEAK, which is constitutively expressed in almost all cell types of the immune system and some non-hematopoietic cell types, is initially synthesized as a type II transmembrane protein, but then secreted as a soluble cytokine due to furin-mediated cleavage (12–14). The Fn14 receptor is expressed at a relatively low level in healthy tissues. The activity of the TWEAK-Fn14 axis is enhanced because of a highly induced local expression of Fn14 in injury, leading to the activation of multiple signaling pathways known to regulate inflammation, angiogenesis, and cell survival, proliferation, migration, and differentiation (8–11, 14).

Accumulating evidence suggests that the TWEAK-Fn14 axis plays an important role in the regulation of skeletal muscle mass and function (4, 13, 15). The activity of the TWEAK/Fn14 axis has also been found to be increased in response to acute muscle injury (16), degenerative muscle diseases such as burn injury (17), myotonic dystrophy (18, 19), amyotrophic lateral sclerosis (20), inclusion-body myositis (21), and spinal cord injury associated muscle atrophy and fibrosis (22). Furthermore, the levels of Fn14 are increased in skeletal muscle in various catabolic conditions, including functional denervation and fasting (23–26). We have previously reported that denervation-induced skeletal muscle atrophy is significantly inhibited in global TWEAK-KO mice and exacerbated in muscle-specific TWEAK-transgenic mice (23). Furthermore, TWEAK-KO mice show considerably reduced fasting-induced muscle atrophy (25). Recently, it was reported that the inhibition of the TWEAK/Fn14 axis augments basal synaptic transmission and protects against synaptic transmission deficits following ischemic stroke (27). Intriguingly, there are also published reports suggesting that Fn14 can regulate some cellular responses independent of TWEAK

cytokine (4, 15). For example, Johnston et al (28) demonstrated that the expression of Fn14 in tumors causes skeletal muscle wasting in a mouse model of cancer cachexia. Furthermore, TWEAK can also engage other receptors, such as CD163, which is expressed in macrophages (29). During tissue ischemia, soluble CD163 (sCD163) functions as a decoy receptor for TWEAK. Genetic ablation of CD163 in mice leads to transiently elevated levels of TWEAK and Notch signaling leading to increased proliferation of muscle progenitor cells and improvement in skeletal muscle regeneration in response to unilateral femoral ligation (29).

Although most of the published reports suggest that the expression of Fn14 is induced in the "settings" of muscle injury or specific atrophy conditions (13), there are other reports suggesting that the gene expression of Fn14 is significantly upregulated in response to exercise training in humans (30–32). The transient increase in the expression of Fn14 in response to resistance or endurance exercise is associated with the activation of markers of the non-canonical NF-κB pathway (30). However, it remains unknown whether Fn14 is induced in the skeletal muscle or other cell types, including blood vessels, present in muscle tissues. Moreover, the physiological significance of the increased expression of Fn14 in skeletal muscle tissues in response to exercise training remains unclear.

To understand the dual role of Fn14 in the regulation of exercise capacity and skeletal muscle mass; in this study, we generated mice with specific deletion of Fn14 in the skeletal muscle. Here, we show that muscle-specific deletion of Fn14 improves exercise capacity and capillary density in the skeletal muscle of mice. Moreover, targeted ablation of Fn14 inhibits denervation-induced skeletal muscle atrophy in mice. Our results also demonstrate that Fn14 regulates the activation of NF-κB and Akt-FOXO signaling in denervated skeletal muscle.

## MATERIALS AND METHODS

### Animals.

Floxed Fn14 (TNFRSF12A, henceforth $Fn14^{fl/fl}$) mice (provided by Biogen, Indc.) were generated by Taconic by inserting loxP sites upstream of exon 2 and downstream of exon 4 of Fn14 as described (33). $Fn14^{fl/fl}$ mice were crossed with muscle creatine kinase (MCK)-Cre (Strain: B6.FVB(129S4)-Tg(Ckmm-cre)5Khn/J, Jackson Laboratory, Bar Harbor, ME) mice to generate muscle-specific Fn14 knockout (henceforth $Fn14^{mKO}$) mice and littermate $Fn14^{fl/fl}$ mice. All mice were of C57BL6/J background and housed in a 12-h light-dark cycle with water and food provided ad libitum. Denervation surgery in mice was performed similar to as described (23). In brief, 10-week-old mice were anaesthetized using isoflurane and the left and right hindquarters were shaved. Finally, a small incision was made to transect around 2 mm of the sciatic nerve. The wound site was closed using surgical glue. The mice were given intraperitoneal injection of carprofen 6h before surgery and two consecutive days after performing denervation surgery. The mice were euthanized on day 3 or 14 post-denervation surgery. All experiments were approved by the Animal Care Operations and the Institutional Animal Care and Use Committee at the University of Houston.

### Metabolic cage analysis.

We employed an Automated Home Cage Phenotyping System (TSE PhenoMaster, Chesterfield, MO) to measure the volume of $O_2$ consumed ($VO_2$) and volume of carbon dioxide produced ($VCO_2$), as well as the whole-body energy expenditure and food and water intake. The system was first calibrated against standard gas mixtures. Finally, individual mice were transferred to an experimental cage containing specialized lids for water and food delivery and inlet/outlet airflow. The mice were acclimatized in the cages for 3 days. The measurement was performed for 24 h at room temperature. Data collected during the light and dark phases were analyzed and used for statistical analysis.

### Grip Strength Measurements.

The total (4-paw) grip strength of mice was measured using a digital grip-strength meter (Columbus Instruments, Columbus, OH, USA) and normalized by total body weight. In brief, mice were acclimatized for 5 min before the beginning of the test. The mouse was allowed to grasp the four-paw pull-bar assembly. The mouse was gently drawn with constant force in a straight line until it could no longer grasp the bar. The force at the time of release was recorded as the peak tension. Each mouse was tested 6 times with a 20–40-s break between tests. The mean peak tension from 6 trials normalized by total body weight was defined as total grip strength.

### In vivo muscle fatigue test.

We used a fatigue protocol where 180 Hz stimulation was given every second for 30 sec for 30 stimuli. The integral force generated during each stimulus was normalized to bodyweight. Contractile events were recorded with the ASI611A Dynamic Muscle Control software (Aurora Scientific) and were calculated with the accompanying ASI611A Dynamic Muscle Analysis software (Aurora Scientific).

### Treadmill running protocol:

Mice were subjected to an acute bout of the treadmill (Eco3/6 treadmill; Columbus Instruments, Columbus, OH) running at 15 m/min for 90 min. All mice in the exercise group finished the 90-min trial and were visibly exhausted. Mice were sacrificed after 6 h to study levels of Fn14 in skeletal muscle.

### Exercise tolerance Test.

The exercise capacity of mice was determined as described (34). In brief, all mice were allowed to run on a rodent treadmill (Columbus Instruments, Columbus, OH, USA) at 10 m/min for 5 min at 0% degree incline for acclimation for 3 days. On the exercise-testing day, the mice were run on the treadmill with a fixed slope of 10%. Mice first ran at 10 m/min for 5 min, and the speed was increased by 1 m/min every 2 min until they were exhausted. The criterion of exhaustion was defined as the inability of mice to run on the treadmill for 10 s despite hand prodding. Running time and maximum speed achieved were measured, and total running distance and work were calculated.

### Histology and morphometric analysis.

Mice were euthanized and tibialis anterior (TA) and soleus muscle were isolated, flash-frozen in liquid nitrogen, mounted in an embedding medium, and sectioned with a microtome cryostat. To assess tissue morphology and measure myofiber cross-sectional area (CSA), 10-μm-thick transverse sections with stained hematoxylin and eosin (H&E) dye. The sections were examined under an inverted microscope (Eclipse TE 2000-U; Nikon) at room temperature with a Plan ×10/0.25 NA Ph1 DL or a Plan Fluor ELWD ×20/0.45 NA Ph1 DM objective lens, a digital camera (Digital Sight DS-Fi1; Nikon), and NIS Elements BR 3.10 software (Nikon). Images of H&E-stained TA or soleus muscle sections were quantified with Fiji software to measure myofiber CSA. The distribution of myofiber CSA was calculated by analyzing ~500 myofibers per muscle.

### Muscle fiber-type immunostaining.

The composition of slow- and fast-type myofibers in TA and soleus muscle was analyzed as described (35). Whole muscle sections were used to quantify the percentage of type I, IIA, IIX, and IIB myosin heavy chain (MyHC) fibers after staining with mAb against type I (clone: BA-D5-c), type IIA (clone: SC-71-c), and type IIB (clone: BF-F3-c) MyHC isoforms (Developmental Studies Hybridoma Bank).

### Succinate dehydrogenase (SDH) staining.

Transverse sections (10 μm) were cut from the mid-belly of the TA muscles on a cryostat at −20°C. The sections were dried at room temperature for 30 min before incubation in a solution made up of 0.2 M phosphate buffer (pH 7.4), 0.1 M MgCl2, 0.2 M succinic acid, and 2.4 mM nitroblue tetrazolium at 37°C in a humidity chamber for 45 min. The sections were then washed in deionized water for 3 min, dehydrated in 50% ethanol for 2 min, and mounted for viewing with DPX mount medium (Electron Microscopy Sciences, Hatfield, PA, USA). Digital photographs were taken from each section at 4X magnification under a Nikon Eclipse TE 2000-U microscope (Nikon, Melville, NY, USA) with a Nikon digital camera (Digital Sight DS-Fi1).

### Immunostaining for CD31.

To analyze the number of capillaries, 10 μm-thick transverse sections of TA and soleus muscle were immunostained for CD31 as previously described (36). Briefly, the sections were by cold acetone for 10 min and dried in air for 30 min. Rinsed with phosphate-buffered saline (PBS) twice, blocked in 2% BSA solution at room temperature for 1 h, followed by incubation with primary antibodies for CD31 and laminin protein at 4°C in a humidity chamber overnight. On the next day, the slides were rinsed with PBS and incubated with a secondary antibody. Nuclei were counterstained with DAPI and the sections were mounted with DPX mounting medium.

### Western blot.

The relative amounts of various proteins were determined by performing Western blot (22). In brief, gastrocnemius (GA) muscle was homogenized in ice-cold lysis buffer [50 mM Tris (pH 8.0), 200 mM NaCl, 50 mM NaF, 0.3% Igepal, 1 mM DTT, 1 mM

sodium orthovanadate, and 100 μM PMSF] supplemented with protease inhibitor cocktail (Thermo Fisher Scientific). The samples were centrifuged at 14 000g for 10 min at 4°C, and the supernatants were collected for subsequent analyses. About 100 μg of protein was resolved on 10%–12% SDS-polyacrylamide gel, blotted onto 0.45 μm nitrocellulose membrane, and probed with a specific primary antibody. Bound antibodies were detected by secondary antibodies conjugated to horseradish peroxidase (Cell Signaling Technology). Signal detection was performed by an ECL detection reagent (Bio-Rad, Hercules, CA, USA). Approximate molecular masses were determined by comparison with the migration of prestained protein standards (Bio-Rad). Finally, band intensities were quantified with ImageJ software.

### RNA isolation and quantitative real-time PCR (qRT-PCR) assay.

Total RNA isolated from skeletal muscle tissues of mice was subjected to reverse transcription and real-time quantitative PCR (qPCR) analysis, as previously described (23).

### Statistical analyses.

Results are expressed as means ± SEM. An unpaired, 2-tailed Student's t test was used to compare quantitative data populations with normal distribution and equal variance, or two-way ANOVA followed by Tukey's multiple comparison test. A value of $p \leq .05$ was considered significant.

## RESULTS

### Targeted ablation of Fn14 improves exercise capacity in adult mice.

We first investigated how the gene expression of Fn14 is regulated in response to exercise. Wild-type mice were subjected to a single acute bout of treadmill exercise. After 6 h, the mice were euthanized and the mRNA levels of Fn14 were measured by performing the qRT-PCR assay. Results showed a significant increase in mRNA levels of Fn14 in the TA muscle of exercised mice compared to corresponding sedentary mice (Figure 1A). To understand the role of Fn14 in the regulation of skeletal muscle mass and function, we crossed $Fn14^{fl/fl}$ mice with MCK-Cre mice to generate muscle-specific Fn14 knockout (i.e. $Fn14^{mKO}$) and littermate control (i.e. $Fn14^{fl/fl}$) mice. Our analysis showed that there was no significant difference in body weight between 8-week-old littermate $Fn14^{fl/fl}$ and $Fn14^{mKO}$ mice (Figure 1B). We also found no significant difference in absolute or normalized four-paw grip strength between $Fn14^{fl/fl}$ and $Fn14^{mKO}$ mice (Figure 1C,D). We next analyzed several aspects of behavior relevant to energy homeostasis by indirect calorimetry. There was no significant difference in the rate of O2 consumption or CO2 production (Figure 1E,F). As a result, there was no significant difference in respiration rate or energy expenditure between $Fn14^{fl/fl}$ and $Fn14^{mKO}$ mice (Figure 1G,H). Food and water intake were also comparable between $Fn14^{fl/fl}$ and $Fn14^{mKO}$ mice (Figure 1I).

Following a treadmill-based exercise tolerance protocol, we next investigated whether muscle-specific ablation of Fn14 has any effect on the exercise capacity of adult mice. Results showed that $Fn14^{mKO}$ mice run for a significantly longer duration and at a higher speed compared to littermate $Fn14^{fl/fl}$ mice (Figure 1J,K). Because $Fn14^{mKO}$ mice kept

running at a higher speed, the difference in the running distance became higher in $Fn14^{mKO}$ mice compared to $Fn14^{fl/fl}$ mice (Figure 1L). As a result, work generated by $Fn14^{mKO}$ mice was significantly higher compared with $Fn14^{fl/fl}$ mice (Figure 1M). We also performed a fatigue test at 180 Hz of stimulation/second for 30 s. Although statistical significance was not observed, we found that the $Fn14^{mKO}$ muscle generated more peak tetanic and integral force compared to $Fn14^{fl/fl}$ muscle over the course of the protocol (Figure 1N,O). Altogether, these results suggest that ablation of Fn14 in skeletal muscle improves exercise capacity and fatigue resistance.

### Targeted deletion of Fn14 improves muscle oxidative phenotype.

To understand the mechanisms responsible for the increased exercise capacity in $Fn14^{mKO}$ mice, we investigated whether there is any difference in the proportion of oxidative and glycolytic myofibers in skeletal muscle of adult $Fn14^{fl/fl}$ and $Fn14^{mKO}$ mice. Transverse muscle sections generated from TA or soleus muscle of littermate $Fn14^{fl/fl}$ and $Fn14^{mKO}$ mice were immunostained with antibodies against MyHC type I (slow, oxidative), IIA (fast oxidative), and IIB (fast, glycolytic). Unstained fibers were considered type IIX. Results showed that there was no significant difference in the proportion of type IIA myofibers in TA; however, the proportion of hybrid fibers (intermediate of type IIA and IIX) and type IIX myofibers was increased whereas the proportion of type IIB myofibers was significantly reduced in TA muscle of $Fn14^{mKO}$ mice compared with $Fn14^{fl/fl}$ mice (Figure 2A,B). Histochemical SDH staining also showed an increase in oxidative myofibers in the TA muscle of $Fn14^{mKO}$ mice compared with $Fn14^{fl/fl}$ mice (Figure 2C). In contrast to the TA muscle, there was no significant difference in the proportion of type I, IIA, IIX, or IIB myofibers in the soleus muscle of $Fn14^{fl/fl}$ and $Fn14^{mKO}$ mice (Figure 2D,E). However, the proportion of myofibers with intermediate staining (type I and IIA or type IIA and IIB) was significantly reduced in the soleus muscle of $Fn14^{mKO}$ mice compared with $Fn14^{fl/fl}$ mice. These results suggest that targeted deletion of Fn14 improves the proportion of oxidative myofibers in the skeletal muscle of mice.

### Targeted deletion of Fn14 increases capillary supply in skeletal muscle of mice.

Increased blood perfusion in skeletal muscle is associated with increased exercise capacity. It is also known that muscle-derived factors affect the angiogenesis program in musculature in a paracrine fashion (37). Our previous work showed that oxidative myofiber type switch, such as observed in Figure 2C, is often associated with a simultaneous increase in muscle capillarity (38, 39). Therefore, we sought to determine whether muscle-specific deletion of Fn14 has any impact on the number of capillaries in the skeletal muscle of mice. Transverse TA muscle sections were immunostained for CD31 (an endothelial cell marker) and laminin protein. Nuclei were counterstained with DAPI (Figure 3A). Interestingly, our results showed that the capillary-to-fiber ratio was significantly increased in $Fn14^{mKO}$ mice compared with $Fn14^{fl/fl}$ mice (Figure 3A,B). Similarly, there was also a significant increase in the capillaries number in the soleus muscle of $Fn14^{mKO}$ compared to $Fn14^{fl/fl}$ mice (Figure 3C). The paracrine angiogenesis program in skeletal muscle is regulated by a number of factors, including angiopoietin (ANG) 1 and 2 and vascular endothelial growth factors (VEGFs) (37). Our QRT-PCR analysis showed that the mRNA levels of ANG1, ANG2, and VEGF receptor (VEGFR) 2 and VEGFR3 were significantly increased in the

skeletal muscle of $Fn14^{mKO}$ mice compared to $Fn14^{fl/fl}$ mice. By contrast, mRNA levels of VEGF A2, VEGF C, and VEGF D remained comparable in the skeletal muscle of $Fn14^{fl/fl}$ and $Fn14^{mKO}$ mice (Figure 3D). Interestingly, we also found that transcript levels of PGC-1α, a master regulator of mitochondrial biogenesis and angiogenic program, were also significantly increased in the skeletal muscle of $Fn14^{mKO}$ mice compared with $Fn14^{fl/fl}$ mice (Figure 3D). These results suggest genetic ablation of Fn14 enhances paracrine angiogenesis in murine skeletal muscle.

### Targeted ablation of Fn14 attenuates denervation-induced muscle atrophy in adult mice.

Levels of Fn14 are increased in denervated skeletal muscle of mice (23, 26). We next investigated whether muscle-specific deletion of Fn14 has any impact on denervation-induced muscle atrophy. Right hind limb muscles of 10-week-old $Fn14^{fl/fl}$ and $Fn14^{mKO}$ mice were subjected to denervation surgery whereas left hind limb muscles were sham-operated. After 14d, the TA, GA, and soleus muscles were isolated and analyzed by morphometric and biochemical methods. Western blot analysis showed that levels of Fn14 protein were drastically increased in denervated GA muscle of $Fn14^{fl/fl}$ mice. By contrast, there was no increase in Fn14 protein levels in the denervated muscle of $Fn14^{mKO}$ mice (Figure 4A). There was no difference in the wet weight of individual innervated hind limb muscles. However, the wet weight of the denervated TA muscle of $Fn14^{mKO}$ mice was significantly higher compared with the denervated TA muscle of littermate $Fn14^{fl/fl}$ mice (Figure 4B). We next generated transverse sections of TA and soleus muscle and performed H&E staining (Figure 4C,D). Our quantitative analysis showed that the proportion of myofibers with a higher cross-sectional area (CSA) was considerably improved in denervated TA or soleus muscle of $Fn14^{mKO}$ mice compared to $Fn14^{fl/fl}$ mice (Figure 4E,F). Indeed, average myofiber CSA was significantly higher in the denervated TA muscle of $Fn14^{mKO}$ mice compared with $Fn14^{fl/fl}$ mice (Figure 4G). Our analysis confirmed that the loss in average myofiber CSA was significantly lower in the denervated TA muscle of $Fn14^{mKO}$ mice compared with $Fn14^{fl/fl}$ mice (Figure 4H). Similarly, we also found that average myofiber CSA was improved in the denervated soleus muscle of $Fn14^{mKO}$ mice compared with $Fn14^{fl/fl}$ mice (Figure 4I). Consequently, percentage loss in soleus muscle CSA in response to denervation was significantly reduced in $Fn14^{mKO}$ mice compared with $Fn14^{fl/fl}$ mice (Figure 4J). Collectively, these results suggest that targeted ablation of Fn14 attenuates denervation-induced muscle atrophy in adult mice.

### Targeted ablation of Fn14 inhibits activation of UPS and autophagy in denervated muscle.

To understand the mechanisms by which ablation of Fn14 inhibits denervation-induced muscle atrophy, we investigated the expression of muscle-specific E3 ubiquitin ligases and markers of autophagy. There was a significant increase in mRNA levels of MAFbx, MuRF1, and MUSA1 in GA muscle at day 3 post-denervation. Interestingly, mRNA levels of MuRF1 and MUSA1 were significantly reduced in the denervated muscle of $Fn14^{mKO}$ mice compared with $Fn14^{fl/fl}$ mice (Figure 5A). By contrast, there was no significant difference in mRNA levels of MAFbx or autophagy markers LC3B, Beclin1, and ATG5 between the denervated muscle of $Fn14^{fl/fl}$ and $Fn14^{mKO}$ mice (Figure 5A).

By performing western blot, we also studied the expression of various markers of UPS and autophagy at 14 days post-denervation. Our analysis showed that protein levels of MuRF1, TRAF6, and LC3B, but not MAFbx, were significantly higher in denervated muscle compared with innervated muscle. Intriguingly, the denervation-induced increase in MuRF1 was significantly reduced in $Fn14^{mKO}$ mice compared with $Fn14^{fl/fl}$ mice (Figure 5B,C). Conversion of soluble *LC3B*-I to lipid-bound *LC3B-II* is associated with the formation of autophagosomes in mammals and has been used as marker to study autophagy in various cell types, including skeletal muscle. Our analysis showed that total levels of LC3B-II protein, as well as the ratio of LC3B-II/LC3B-I, were significantly reduced in the denervated muscle of $Fn14^{mKO}$ mice compared to $Fn14^{fl/fl}$ mice (Figure 5B,C). A recently published report suggests that MuRF1 mediates the ubiquitination of thick and thin filament proteins, such as Tropomyosin and Troponin (40). Since the levels of MuRF1 were reduced in the denervated muscle of $Fn14^{mKO}$ mice, we investigated whether the levels of Tropomyosin and Troponin are affected in the denervated muscle of $Fn14^{fl/fl}$ and $Fn14^{mKO}$ mice. Troponin and Tropomyosin protein levels were significantly higher in the denervated GA muscle of $Fn14^{mKO}$ mice compared with $Fn14^{fl/fl}$ mice (Figure 5B,C). Taken together, these results suggest that Fn14-mediated signaling induces muscle proteolysis in denervated muscle potentially through the activation of UPS and autophagy.

## Fn14 regulates the activation of non-canonical NF-κB pathway in denervated skeletal muscle.

NF-κB is a major transcription factor that regulates the gene expression of a plethora of molecules, including those involved in muscle proteolysis (3). By performing western blot, we measured the levels of phosphorylated and total p65 protein (a marker of canonical NF-κB signaling) and p100/p52 protein (markers of non-canonical NF-κB) in innervated and denervated GA muscle of $Fn14^{fl/fl}$ and $Fn14^{mKO}$ mice. There was no significant difference in the levels of phosphorylated p65 (p-p65) or total p65 protein in the denervated muscle of $Fn14^{mKO}$ mice compared with $Fn14^{fl/fl}$ mice (Figure 6A,B). Interestingly, we found that the levels of both p100 and p52 protein were drastically increased in skeletal muscle in response to denervation. Importantly, the denervation-induced increase in the levels of p100 was significantly reduced in $Fn14^{mKO}$ mice compared with $Fn14^{fl/fl}$ mice. By contrast, there was no significant difference in levels of p52 protein between $Fn14^{fl/fl}$ and $Fn14^{mKO}$ mice (Figure 6A,B). We also found that the levels of TRAF2 protein, an upstream activator of NF-κB signaling (3), were significantly reduced in the denervated GA muscle of $Fn14^{mKO}$ mice compared with $Fn14^{fl/fl}$ mice (Figure 6A,B). These results suggest that Fn14 mediates the activation of non-canonical NF-κB signaling in denervated skeletal muscle.

## Targeted ablation of Fn14 inhibits the activation of FOXO transcription factor.

Forkhead box subfamily O (FOXO) transcription factors, such as FoxO1, FoxO3a, and FoxO4 stimulate muscle atrophy by augmenting the gene expression of various components of UPS and autophagy (2). Akt and other kinases phosphorylate FOXO factors at three conserved residues, which results in their export from the nucleus to the cytoplasm, thereby inhibiting FOXO-dependent transcription of atrogenes (2, 6). We next investigated whether genetic ablation of Fn14 affects the phosphorylation of Akt and FOXO factors in the denervated skeletal muscle of mice. Results showed that there was a significant increase in

the levels of phosphorylated as well as total Akt levels in the denervated muscle of $Fn14^{mKO}$ mice compared to their contralateral undenervated muscle (Figure 7A,B). Protein levels of phosphorylated and total mTOR protein were significantly increased in the denervated muscle of both $Fn14^{fl/fl}$ and $Fn14^{mKO}$ mice. However, there was no significant difference in the levels of p-mTOR or total mTOR in the denervated muscle of $Fn14^{fl/fl}$ and $Fn14^{mKO}$ mice (Figure 7A,B).

Western blot analysis showed that the levels of p-FoxO1 and total FoxO1 and Foxo3a protein were increased in the denervated muscle. However, there was no significant difference in p-FoxO1 levels in the denervated GA muscle of $Fn14^{fl/fl}$ and $Fn14^{mKO}$ mice. Total FoxO1 protein levels were significantly higher in the denervated muscle of $Fn14^{mKO}$ mice compared to $Fn14^{fl/fl}$ mice (Figure 7A,B). In addition, levels of p-FoxO3a protein were significantly higher in denervated GA muscle of $Fn14^{mKO}$ mice compared to $Fn14^{fl/fl}$ mice. By contrast, levels of p-FoxO4 protein decreased after denervation in both $Fn14^{fl/fl}$ and $Fn14^{mKO}$ mice. Interestingly, the levels of p-FoxO4 protein were significantly reduced in the innervated muscle of $Fn14^{mKO}$ mice compared to the corresponding innervated muscle of $Fn14^{fl/fl}$ mice (Figure 7A,B). Taken together, these results suggest that Fn14 regulates the phosphorylation of Akt and FOXO transcription factors in the denervated skeletal muscle of mice.

## DISCUSSION

Proinflammatory cytokines play an important role in the regulation of myogenesis and skeletal muscle mass in various physiological and pathophysiological conditions (1–3). Consistently, the TWEAK-Fn14 system has been found to regulate various aspects of skeletal muscle physiology. Earlier studies showed that a high concentration of recombinant TWEAK protein induces the proliferation of cultured myoblasts but inhibits their differentiation into multinucleated myotubes potentially through the sustained activation of the canonical NF-κB signaling pathway and degradation of MyoD protein (41, 42). TWEAK also inhibits the self-renewal of satellite cells both in vitro and in vivo (43). By contrast, low amounts of recombinant TWEAK protein promote myoblast fusion leading to the formation of larger size myotubes. These effects of low concentrations of TWEAK on myoblast fusion are attributed to its ability to activate non-canonical NF-κB signaling which promotes myoblast fusion (44). Previous studies have also shown that muscle regeneration is delayed in global Fn14-knockout mice potentially due to a reduction in initial immune response (i.e. recruitment of monocytes and neutrophils), which is needed for the removal of tissue debris after muscle damage (42, 45). While low levels of TWEAK induce myoblast proliferation and fusion, overstimulation of the Fn14 receptor by TWEAK that occurs in various muscle degenerative diseases results in the inhibition of muscle regeneration (4, 13, 17, 18). Indeed, transgenic overexpression of TWEAK (a model of chronic supraphysiological levels of TWEAK in skeletal muscle) inhibits muscle regeneration in mice. Conversely, muscle regeneration is slightly improved in TWEAK-KO mice (16).

Since low levels of TWEAK augments myoblast proliferation and fusion, a few studies have suggested that the increase in the levels of TWEAK and/or Fn14 in the skeletal muscle is an adaptive myogenic response (15). Indeed, the mRNA levels of Fn14 are transiently increased

in muscle biopsies following resistance or running exercise (30–32). Our results in this study also show a significant increase in transcript levels of Fn14 in the skeletal muscle of mice after a bout of treadmill exercise (Figure 1A). However, the physiological significance of this transient increase in Fn14 levels in skeletal muscle remains unknown. In this study, we generated mice in which Fn14 was specifically deleted in skeletal muscle. Similar to global Fn14-KO mice, we did not find any difference in skeletal muscle mass, myofiber CSA, or grip strength between control and muscle-specific Fn14-KO mice suggesting that Fn14 has no role in development of skeletal muscle during embryogenesis (Figure 1). Interestingly, we found that ablation of Fn14 in the skeletal muscle significantly improved exercise tolerance in adult mice. Moreover, the skeletal muscle of $Fn14^{mKO}$ mice is more resistant to fatigue in response to chronic stimulation (Figure 1). These results suggest that muscle Fn14 has a somewhat negative impact on the regulation of exercise capacity. It is notable that exercise training induces mild muscle injury and associated inflammatory response (46). Therefore, it is possible that an increase in Fn14 levels in skeletal muscle tissues after resistance or run exercise (30–32) could also be attributed to its expression in inflammatory immune cells or satellite cells. Furthermore, it remains to be seen whether $Fn14^{mKO}$ mice undergo enhanced adaptation to long-term exercise training compared to wild type mice. Our results on untrained mice suggest that this might be the case.

Myofibers are classified into type I, IIA, IIX, and IIB based on the expression of specific myosin heavy chain (MHC) isoforms. Types I and IIA myofibers exhibit oxidative metabolic phenotypes, whereas type IIB are primarily glycolytic. Type IIX myofibers are uniquely fast-twitch yet with high oxidative capacity. Oxidative myofibers generally are rich in mitochondria, and also have more capillary density compared to glycolytic myofibers (47). Compared to type IIB myofibers, type I, IIA, and also IIX myofibers exhibit a high resistance to fatigue and are necessary for endurance (47). Improvement in exercise capacity is generally associated with the transition to type IIX/IIA/I myofibers in skeletal muscle. Our histological analysis showed that muscle-specific deletion of Fn14 increases the proportion of type IIX myofibers and significantly decreases type IIb myofibers in the TA muscle of mice. In the soleus muscle, there was no difference in the proportion of type I, IIA, IIX, or IIB except that hybrid myofibers were significantly reduced in $Fn14^{mKO}$ mice compared with $Fn14^{fl/fl}$ mice (Figure 2). In addition, we found a significant increase in the number of capillaries per myofiber in $Fn14^{mKO}$ mice, which could be attributed to increased expression of ANG1, ANG2, VEGF receptors, and PGC-1α (Figure 3). Notably, PGC1α is a key transcriptional master regulator of oxidative metabolism, angiogenesis, and vascularization in the skeletal muscle, and its increased expression is associated with improved exercise capacity (48–50). While more investigations are needed to understand the mechanisms of action of Fn14 in skeletal muscle, an increased proportion of oxidative myofibers and a higher number of capillaries surrounding myofibers may be responsible for the improvement in exercise capacity and resistance to fatigue in $Fn14^{mKO}$ mice. Although to a much lesser extent compared to skeletal muscle, the MCK-Cre line used in this study can also delete floxed Fn14 allele in cardiomyocytes (51). Therefore, the depletion of Fn14 levels in cardiac tissue could be another potential mechanism for the improvement of exercise capacity in $Fn14^{mKO}$ mice.

The TWEAK-Fn14 axis has been found to be an important mediator of muscle wasting in many conditions (13, 15). We have previously reported that transgenic overexpression of TWEAK in the skeletal muscle of mice causes atrophy whereas global TWEAK-KO mice show significantly reduced muscle atrophy in response to denervation (23). Importantly, the expression of TWEAK receptor Fn14, but not TWEAK itself, is increased in skeletal muscle in various catabolic states (13, 23, 26). However, it remained unknown whether inhibition of Fn14 is sufficient to rescue muscle wasting in various catabolic states. A recent study demonstrated that Fn14 expression in tumors causes skeletal muscle wasting in a mouse model of cancer cachexia (28). While the study showed that Fn14 overexpression in tumors causes cachexia, it could not dissect the role of Fn14 in muscle during cachexia. A change in Fn14 expression in the tumor itself could alter the cytokine milieu and tumor-derived factors, which can affect muscle differently. Our results in the present study demonstrate that targeted deletion of Fn14 significantly reduces denervation-induced muscle wasting in adult mice and hence provides the muscle role of Fn14 in neurogenic atrophy (Figure 4).

The UPS and autophagy are two major proteolytic systems, which stimulate protein degradation in atrophying skeletal muscle (2). The expression of many E3 ubiquitin ligases, such as MAFbx, MuRF1, MUSA1, and TRAF6 is increased in skeletal muscle in various atrophy conditions leading to the increased degradation of thick and thin filament proteins (6, 40, 52–54). Results of the present investigation show that Fn14-mediated signaling induces the expression of MuRF1 and MUSA1 in 3d-denervated skeletal muscle. The levels of MuRF1 remained low in the skeletal muscle of $Fn14^{mKO}$ mice even after 14 days of denervation. In addition, we found that there was no reduction in the levels of Tropomyosin and Troponin protein in the denervated muscle of $Fn14^{mKO}$ mice suggesting that the inhibition of MuRF1 could be an important mechanism for the reduced muscle proteolysis in $Fn14^{mKO}$ mice following denervation. Furthermore, our results showed that the ratio of LC3B-II/I protein is also reduced in 14d-denervated skeletal muscle of $Fn14^{mKO}$ mice indicating inhibition of autophagy (Figure 5). These results suggest that Fn14-mediated signaling causes denervation-induced muscle atrophy through the activation of the UPS and autophagy.

Skeletal muscle wasting involves the activation of various transcription factors, such as NF-κB and FOXOs, which augment the expression of components of the UPS and autophagy (2). NF-κB transcription factor can be activated through a canonical pathway, which involves upstream activation of inhibitor of kappa B (IκB) kinase (IKK)-β, degradation of IκB protein, and nuclear translocation of p65/p50 dimers. The non-canonical NF-κB signaling involves the activation of IKKα, phosphorylation, and proteolytic processing of p100 protein into p52 protein followed by translocation of p52/RelB dimers to nuclei (3). Published reports demonstrate that the activation of either canonical or non-canonical NF-κB signaling can lead to skeletal muscle wasting in various conditions, including denervation (3, 55–57). While no major difference was noticeable in levels of phosphorylated p65 protein, we observed a drastic reduction in the levels of p100 protein in denervated skeletal muscle of $Fn14^{mKO}$ mice (Figure 6). These results are consistent with previously published reports that in addition to the canonical NF-κB pathway, the TWEAK-Fn14 axis also stimulates non-canonical NF-κB signaling in skeletal muscle (4, 44).

FOXO family of transcription factors, such as FoxO1, FoxO3a, and FoxO4 are the major regulators of skeletal muscle wasting. These factors augment the gene expression of muscle-specific E3 ubiquitin ligases, such as MAFbx, MuRF1, and MUSA1 and stimulate autophagy in skeletal muscle.2 Akt and other kinases phosphorylate FOXO at key residues, which results in the export of FOXOs from the nucleus and their sequestration into the cytoplasm (2). Indeed, the phosphorylation by Akt is a major mechanism for the inhibition of FOXO transcription factors (1, 6). Our results demonstrate that total, as well as phosphorylated levels of Akt, are significantly increased in the denervated skeletal muscle of $Fn14^{mKO}$ mice. Moreover, we also observed a significant increase in the levels of phosphorylated FoxO3a in the denervated muscle of $Fn14^{mKO}$ mice (Figure 7). Although the exact mechanisms remain unknown, repression in the activation of non-canonical NF-κB and FoxO3a transcription factors may be some of the important mechanisms for the reduced muscle atrophy observed in $Fn14^{mKO}$ mice in response to denervation. It is notable that while NF-κB was inhibited, there was no effect on the activation of Akt/FOXO signaling or autophagy in the denervated muscle of wild-type and TWEAK-KO mice (23). These results suggest that TWEAK and Fn14 can regulate denervation-induced muscle atrophy through some distinct mechanisms.

In summary, our study demonstrates that suppression of Fn14 in the skeletal muscle improves exercise capacity and inhibits denervation-induced muscle wasting. Because Fn14 is exclusively expressed and elevated in skeletal muscle under conditions of atrophy, targeting Fn14 could be a promising approach for the prevention of skeletal muscle wasting in future therapies.

## ACKNOWLEDGMENTS.

We are grateful to Dr. Linda C. Burkly of Biogen, Inc. for providing floxed Fn14 mice.

**FUNDING INFORMATION:**

This work was supported by National Institutes of Health grants AR059810 and AR068313 to AK.

## DATA AVAILABILITY STATEMENT.

All the data produced during the experiments of the present manuscript (western blots, microscope images, electrophysiological recordings, primers sequence, and antibody information) are available upon request to the first author and corresponding author.

## ABBREVIATIONS

| | |
|---|---|
| **ANG** | angiopoietin |
| **CSA** | Cross-sectional area |
| **Fn14** | Fibroblast growth factor-inducible 14 |
| **FOXO** | Forkhead box transcription factor O |
| **GA** | gastrocnemius |

| | |
|---|---|
| **H&E** | Hematoxylin and Eosin |
| **MyHC** | Myosin heavy chain |
| **KO** | Knockout |
| **mKO** | muscle KO |
| **NF-κB** | Nuclear factor-kappa B |
| **PGC-1α** | Peroxisome proliferator-activated receptor-gamma coactivator-1alpha |
| **qRT-PCR** | Quantitative real-time polymerase chain reaction |
| **TA** | Tibialis Anterior |
| **TNF** | Tumor Necrosis Factor |
| **TNFRSF12A** | TNF receptor superfamily 12A |
| **TWEAK** | TNF-like weak inducer of apoptosis |
| **SEM** | standard error of the mean |
| **SDH** | Succinate dehydrogenase |
| **UPS** | ubiquitin-proteasome system |
| **VEGF** | vascular endothelial growth factor |
| **VEGFR** | VEGF receptor |

## REFERENCES


1. Bonaldo P, and Sandri M (2013) Cellular and molecular mechanisms of muscle atrophy. Dis Model Mech 6, 25–39 [PubMed: 23268536]
2. Sartori R, Romanello V, and Sandri M (2021) Mechanisms of muscle atrophy and hypertrophy: implications in health and disease. Nat Commun 12, 330 [PubMed: 33436614]
3. Li H, Malhotra S, and Kumar A (2008) Nuclear factor-kappa B signaling in skeletal muscle atrophy. J Mol Med (Berl) 86, 1113–1126 [PubMed: 18574572]
4. Sato S, Ogura Y, and Kumar A (2014) TWEAK/Fn14 Signaling Axis Mediates Skeletal Muscle Atrophy and Metabolic Dysfunction. Front Immunol 5, 18 [PubMed: 24478779]
5. Baehr LM, Hughes DC, Waddell DS, and Bodine SC (2022) SnapShot: Skeletal muscle atrophy. Cell 185, 1618–1618 e1611 [PubMed: 35487192]
6. Sandri M (2013) Protein breakdown in muscle wasting: role of autophagy-lysosome and ubiquitin-proteasome. Int J Biochem Cell Biol 45, 2121–2129 [PubMed: 23665154]
7. Sartori R, Hagg A, Zampieri S, Armani A, Winbanks CE, Viana LR, Haidar M, Watt KI, Qian H, Pezzini C, Zanganeh P, Turner BJ, Larsson A, Zanchettin G, Pierobon ES, Moletta L, Valmasoni M, Ponzoni A, Attar S, Da Dalt G, Sperti C, Kustermann M, Thomson RE, Larsson L, Loveland KL, Costelli P, Megighian A, Merigliano S, Penna F, Gregorevic P, and Sandri M (2021) Perturbed BMP signaling and denervation promote muscle wasting in cancer cachexia. Sci Transl Med 13
8. Chicheportiche Y, Bourdon PR, Xu H, Hsu YM, Scott H, Hession C, Garcia I, and Browning JL (1997) TWEAK, a new secreted ligand in the tumor necrosis factor family that weakly induces apoptosis. J Biol Chem 272, 32401–32410 [PubMed: 9405449]

9. Meighan-Mantha RL, Hsu DK, Guo Y, Brown SA, Feng SL, Peifley KA, Alberts GF, Copeland NG, Gilbert DJ, Jenkins NA, Richards CM, and Winkles JA (1999) The mitogen-inducible Fn14 gene encodes a type I transmembrane protein that modulates fibroblast adhesion and migration. J Biol Chem 274, 33166–33176 [PubMed: 10551889]
10. Winkles JA, Tran NL, Brown SA, Stains N, Cunliffe HE, and Berens ME (2007) Role of TWEAK and Fn14 in tumor biology. Front Biosci 12, 2761–2771 [PubMed: 17127278]
11. Wiley SR, Cassiano L, Lofton T, Davis-Smith T, Winkles JA, Lindner V, Liu H, Daniel TO, Smith CA, and Fanslow WC (2001) A novel TNF receptor family member binds TWEAK and is implicated in angiogenesis. Immunity 15, 837–846 [PubMed: 11728344]
12. Zheng TS, and Burkly LC (2008) No end in site: TWEAK/Fn14 activation and autoimmunity associated- end-organ pathologies. J Leukoc Biol 84, 338–347 [PubMed: 18483204]
13. Tajrishi MM, Zheng TS, Burkly LC, and Kumar A (2014) The TWEAK-Fn14 pathway: a potent regulator of skeletal muscle biology in health and disease. Cytokine Growth Factor Rev 25, 215–225 [PubMed: 24444596]
14. Burkly LC (2014) TWEAK/Fn14 axis: the current paradigm of tissue injury-inducible function in the midst of complexities. Semin Immunol 26, 229–236 [PubMed: 24636536]
15. Pascoe AL, Johnston AJ, and Murphy RM (2020) Controversies in TWEAK-Fn14 signaling in skeletal muscle atrophy and regeneration. Cell Mol Life Sci 77, 3369–3381 [PubMed: 32200423]
16. Mittal A, Bhatnagar S, Kumar A, Paul PK, Kuang S, and Kumar A (2010) Genetic ablation of TWEAK augments regeneration and post-injury growth of skeletal muscle in mice. Am J Pathol 177, 1732–1742 [PubMed: 20724600]
17. Merritt EK, Thalacker-Mercer A, Cross JM, Windham ST, Thomas SJ, and Bamman MM (2013) Increased expression of atrogenes and TWEAK family members after severe burn injury in nonburned human skeletal muscle. J Burn Care Res 34, e297–304 [PubMed: 23816995]
18. Yadava RS, Foff EP, Yu Q, Gladman JT, Kim YK, Bhatt KS, Thornton CA, Zheng TS, and Mahadevan MS (2015) TWEAK/Fn14, a pathway and novel therapeutic target in myotonic dystrophy. Hum Mol Genet 24, 2035–2048 [PubMed: 25504044]
19. Yadava RS, Foff EP, Yu Q, Gladman JT, Zheng TS, and Mahadevan MS (2016) TWEAK Regulates Muscle Functions in a Mouse Model of RNA Toxicity. PLoS One 11, e0150192 [PubMed: 26901467]
20. Bowerman M, Salsac C, Coque E, Eiselt E, Deschaumes RG, Brodovitch A, Burkly LC, Scamps F, and Raoul C (2015) Tweak regulates astrogliosis, microgliosis and skeletal muscle atrophy in a mouse model of amyotrophic lateral sclerosis. Hum Mol Genet 24, 3440–3456 [PubMed: 25765661]
21. Morosetti R, Gliubizzi C, Sancricca C, Broccolini A, Gidaro T, Lucchini M, and Mirabella M (2012) TWEAK in inclusion-body myositis muscle: possible pathogenic role of a cytokine inhibiting myogenesis. Am J Pathol 180, 1603–1613 [PubMed: 22314077]
22. Yarar-Fisher C, Bickel CS, Kelly NA, Stec MJ, Windham ST, McLain AB, Oster RA, and Bamman MM (2016) Heightened TWEAK-NF-kappaB signaling and inflammation-associated fibrosis in paralyzed muscles of men with chronic spinal cord injury. Am J Physiol Endocrinol Metab 310, E754–761 [PubMed: 26931128]
23. Mittal A, Bhatnagar S, Kumar A, Lach-Trifilieff E, Wauters S, Li H, Makonchuk DY, Glass DJ, and Kumar A (2010) The TWEAK–Fn14 system is a critical regulator of denervation-induced skeletal muscle atrophy in mice. J Cell Biol 188, 833–849 [PubMed: 20308426]
24. Hindi SM, Mishra V, Bhatnagar S, Tajrishi MM, Ogura Y, Yan Z, Burkly LC, Zheng TS, and Kumar A (2014) Regulatory circuitry of TWEAK-Fn14 system and PGC-1alpha in skeletal muscle atrophy program. FASEB J 28, 1398–1411 [PubMed: 24327607]
25. Paul PK, Bhatnagar S, Mishra V, Srivastava S, Darnay BG, Choi Y, and Kumar A (2012) The E3 ubiquitin ligase TRAF6 intercedes in starvation-induced skeletal muscle atrophy through multiple mechanisms. Mol Cell Biol 32, 1248–1259 [PubMed: 22290431]
26. Tajrishi MM, Shin J, Hetman M, and Kumar A (2014) DNA methyltransferase 3a and mitogen-activated protein kinase signaling regulate the expression of fibroblast growth factor-inducible 14 (Fn14) during denervation-induced skeletal muscle atrophy. J Biol Chem 289, 19985–19999 [PubMed: 24895120]

27. Nagy D, Ennis KA, Wei R, Su SC, Hinckley CA, Gu RF, Gao B, Massol RH, Ehrenfels C, Jandreski L, Thomas AM, Nelson A, Gyoneva S, Hajos M, and Burkly LC (2021) Developmental synaptic regulator, TWEAK/Fn14 signaling, is a determinant of synaptic function in models of stroke and neurodegeneration. Proc Natl Acad Sci U S A 118

28. Johnston AJ, Murphy KT, Jenkinson L, Laine D, Emmrich K, Faou P, Weston R, Jayatilleke KM, Schloegel J, Talbo G, Casey JL, Levina V, Wong WW, Dillon H, Sahay T, Hoogenraad J, Anderton H, Hall C, Schneider P, Tanzer M, Foley M, Scott AM, Gregorevic P, Liu SY, Burkly LC, Lynch GS, Silke J, and Hoogenraad NJ (2015) Targeting of Fn14 Prevents Cancer-Induced Cachexia and Prolongs Survival. Cell 162, 1365–1378 [PubMed: 26359988]

29. Akahori H, Karmali V, Polavarapu R, Lyle AN, Weiss D, Shin E, Husain A, Naqvi N, Van Dam R, Habib A, Choi CU, King AL, Pachura K, Taylor WR, Lefer DJ, and Finn AV (2015) CD163 interacts with TWEAK to regulate tissue regeneration after ischaemic injury. Nat Commun 6, 7792 [PubMed: 26242746]

30. Raue U, Jemiolo B, Yang Y, and Trappe S (2015) TWEAK-Fn14 pathway activation after exercise in human skeletal muscle: insights from two exercise modes and a time course investigation. J Appl Physiol (1985) 118, 569–578 [PubMed: 25539934]

31. Murach K, Raue U, Wilkerson B, Minchev K, Jemiolo B, Bagley J, Luden N, and Trappe S (2014) Single muscle fiber gene expression with run taper. PLoS One 9, e108547 [PubMed: 25268477]

32. Raue U, Trappe TA, Estrem ST, Qian HR, Helvering LM, Smith RC, and Trappe S (2012) Transcriptome signature of resistance exercise adaptations: mixed muscle and fiber type specific profiles in young and old adults. J Appl Physiol (1985) 112, 1625–1636 [PubMed: 22302958]

33. Gupta RK, Gracias DT, Figueroa DS, Miki H, Miller J, Fung K, Ay F, Burkly L, and Croft M (2021) TWEAK functions with TNF and IL-17 on keratinocytes and is a potential target for psoriasis therapy. Sci Immunol 6, eabi8823

34. Sato S, Ogura Y, Tajrishi MM, and Kumar A (2015) Elevated levels of TWEAK in skeletal muscle promote visceral obesity, insulin resistance, and metabolic dysfunction. FASEB J 29, 988–1002 [PubMed: 25466899]

35. Hindi SM, Sato S, Xiong G, Bohnert KR, Gibb AA, Gallot YS, McMillan JD, Hill BG, Uchida S, and Kumar A (2018) TAK1 regulates skeletal muscle mass and mitochondrial function. JCI Insight 3

36. Sato S, Ogura Y, Mishra V, Shin J, Bhatnagar S, Hill BG, and Kumar A (2013) TWEAK promotes exercise intolerance by decreasing skeletal muscle oxidative phosphorylation capacity. Skelet Muscle 3, 18 [PubMed: 23835416]

37. Kumar A, and Narkar VA (2022) Nuclear receptors as potential therapeutic targets in peripheral arterial disease and related myopathy. FEBS J, doi: 10.1111/febs.16593.

38. Narkar VA, Fan W, Downes M, Yu RT, Jonker JW, Alaynick WA, Banayo E, Karunasiri MS, Lorca S, and Evans RM (2011) Exercise and PGC-1alpha-independent synchronization of type I muscle metabolism and vasculature by ERRgamma. Cell Metab 13, 283–293 [PubMed: 21356518]

39. Sopariwala DH, Likhite N, Pei G, Haroon F, Lin L, Yadav V, Zhao Z, and Narkar VA (2021) Estrogen-related receptor alpha is involved in angiogenesis and skeletal muscle revascularization in hindlimb ischemia. FASEB J 35, e21480 [PubMed: 33788962]

40. Baehr LM, Hughes DC, Lynch SA, Van Haver D, Maia TM, Marshall AG, Radoshevich L, Impens F, Waddell DS, and Bodine SC (2021) Identification of the MuRF1 Skeletal Muscle Ubiquitylome Through Quantitative Proteomics. Function (Oxf) 2, zqab029

41. Dogra C, Changotra H, Mohan S, and Kumar A (2006) Tumor necrosis factor-like weak inducer of apoptosis inhibits skeletal myogenesis through sustained activation of nuclear factor-kappaB and degradation of MyoD protein. J Biol Chem 281, 10327–10336 [PubMed: 16461349]

42. Girgenrath M, Weng S, Kostek CA, Browning B, Wang M, Brown SA, Winkles JA, Michaelson JS, Allaire N, Schneider P, Scott ML, Hsu YM, Yagita H, Flavell RA, Miller JB, Burkly LC, and Zheng TS (2006) TWEAK, via its receptor Fn14, is a novel regulator of mesenchymal progenitor cells and skeletal muscle regeneration. EMBO J 25, 5826–5839 [PubMed: 17124496]

43. Ogura Y, Mishra V, Hindi SM, Kuang S, and Kumar A (2013) Proinflammatory cytokine tumor necrosis factor (TNF)-like weak inducer of apoptosis (TWEAK) suppresses satellite cell self-

renewal through inversely modulating Notch and NF-kappaB signaling pathways. J Biol Chem 288, 35159–35169 [PubMed: 24151074]

44. Enwere EK, Holbrook J, Lejmi-Mrad R, Vineham J, Timusk K, Sivaraj B, Isaac M, Uehling D, Al-awar R, LaCasse E, and Korneluk RG (2012) TWEAK and cIAP1 regulate myoblast fusion through the noncanonical NF-kappaB signaling pathway. Science signaling 5, ra75
45. Tidball JG (2017) Regulation of muscle growth and regeneration by the immune system. Nat Rev Immunol 17, 165–178 [PubMed: 28163303]
46. Clarkson PM, and Hubal MJ (2002) Exercise-induced muscle damage in humans. Am J Phys Med Rehabil 81, S52–69 [PubMed: 12409811]
47. Schiaffino S, and Reggiani C (1996) Molecular diversity of myofibrillar proteins: gene regulation and functional significance. Physiol Rev 76, 371–423 [PubMed: 8618961]
48. Lin J, Wu H, Tarr PT, Zhang CY, Wu Z, Boss O, Michael LF, Puigserver P, Isotani E, Olson EN, Lowell BB, Bassel-Duby R, and Spiegelman BM (2002) Transcriptional co-activator PGC-1 alpha drives the formation of slow-twitch muscle fibres. Nature 418, 797–801 [PubMed: 12181572]
49. Calvo JA, Daniels TG, Wang X, Paul A, Lin J, Spiegelman BM, Stevenson SC, and Rangwala SM (2008) Muscle-specific expression of PPARgamma coactivator-1alpha improves exercise performance and increases peak oxygen uptake. J Appl Physiol (1985) 104, 1304–1312 [PubMed: 18239076]
50. Arany Z, Foo SY, Ma Y, Ruas JL, Bommi-Reddy A, Girnun G, Cooper M, Laznik D, Chinsomboon J, Rangwala SM, Baek KH, Rosenzweig A, and Spiegelman BM (2008) HIF-independent regulation of VEGF and angiogenesis by the transcriptional coactivator PGC-1alpha. Nature 451, 1008–1012 [PubMed: 18288196]
51. Bruning JC, Michael MD, Winnay JN, Hayashi T, Horsch D, Accili D, Goodyear LJ, and Kahn CR (1998) A muscle-specific insulin receptor knockout exhibits features of the metabolic syndrome of NIDDM without altering glucose tolerance. Mol Cell 2, 559–569 [PubMed: 9844629]
52. Bodine SC, Latres E, Baumhueter S, Lai VK, Nunez L, Clarke BA, Poueymirou WT, Panaro FJ, Na E, Dharmarajan K, Pan ZQ, Valenzuela DM, DeChiara TM, Stitt TN, Yancopoulos GD, and Glass DJ (2001) Identification of ubiquitin ligases required for skeletal muscle atrophy. Science 294, 1704–1708 [PubMed: 11679633]
53. Sartori R, Schirwis E, Blaauw B, Bortolanza S, Zhao J, Enzo E, Stantzou A, Mouisel E, Toniolo L, Ferry A, Stricker S, Goldberg AL, Dupont S, Piccolo S, Amthor H, and Sandri M (2013) BMP signaling controls muscle mass. Nat Genet 45, 1309–1318 [PubMed: 24076600]
54. Clarke BA, Drujan D, Willis MS, Murphy LO, Corpina RA, Burova E, Rakhilin SV, Stitt TN, Patterson C, Latres E, and Glass DJ (2007) The E3 Ligase MuRF1 degrades myosin heavy chain protein in dexamethasone-treated skeletal muscle. Cell Metab 6, 376–385 [PubMed: 17983583]
55. Cai D, Frantz JD, Tawa NE Jr., Melendez PA, Oh BC, Lidov HG, Hasselgren PO, Frontera WR, Lee J, Glass DJ, and Shoelson SE (2004) IKKbeta/NF-kappaB activation causes severe muscle wasting in mice. Cell 119, 285–298 [PubMed: 15479644]
56. Van Gammeren D, Damrauer JS, Jackman RW, and Kandarian SC (2009) The IkappaB kinases IKKalpha and IKKbeta are necessary and sufficient for skeletal muscle atrophy. FASEB J 23, 362–370 [PubMed: 18827022]
57. Wu CL, Cornwell EW, Jackman RW, and Kandarian SC (2014) NF-kappaB but not FoxO sites in the MuRF1 promoter are required for transcriptional activation in disuse muscle atrophy. Am J Physiol Cell Physiol 306, C762–767 [PubMed: 24553183]

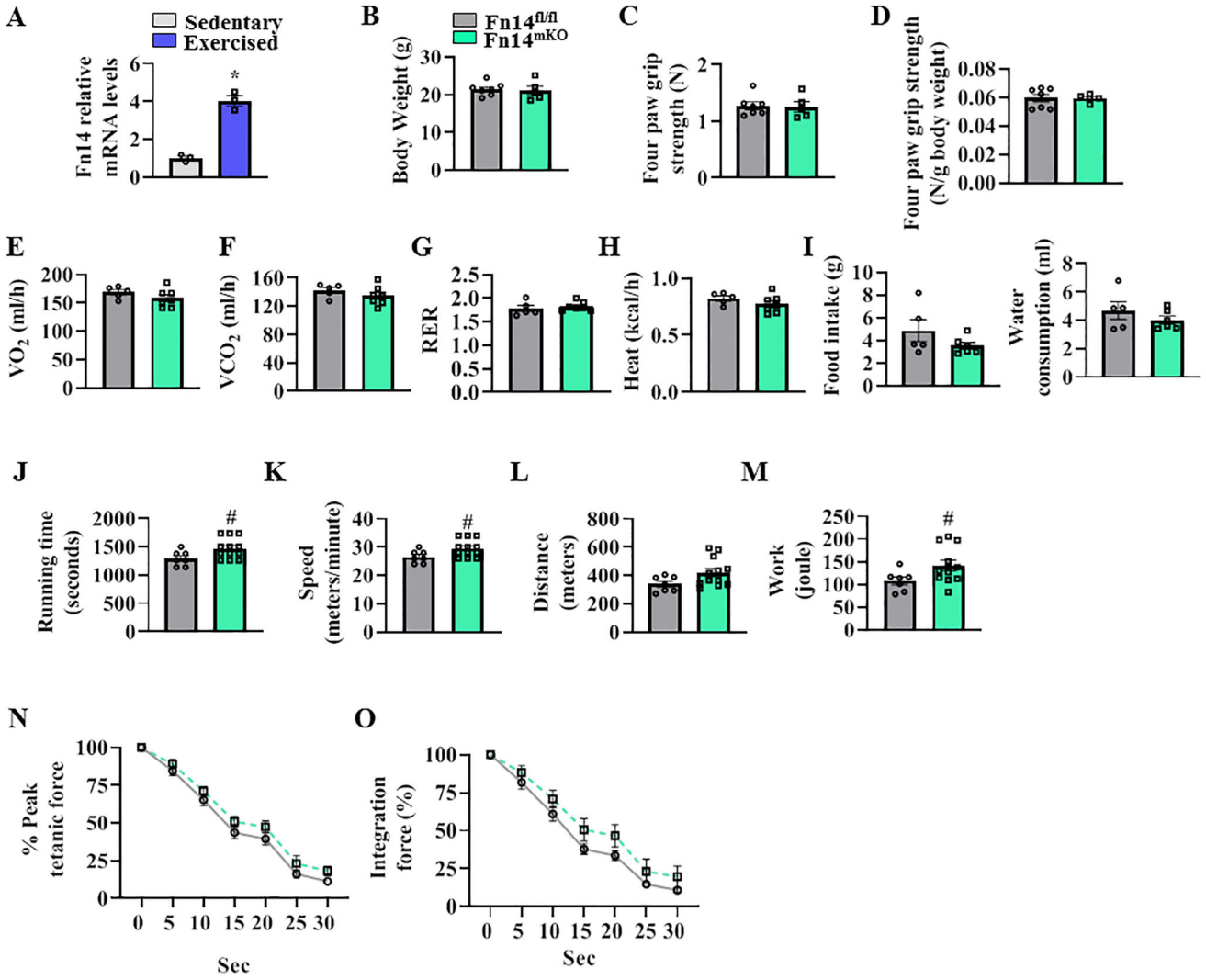


**FIGURE 1. Effect of muscle-specific ablation of Fn14 on exercise capacity of mice.**

(A) Transcript levels of Fn14 in TA muscle of sedentary and exercised wild-type mice. $n = 3$ in each group. $*p < .05$, values significantly different from sedentary mice by unpaired t-test. (B) Average body weight of littermate $Fn14^{fl/fl}$ and $Fn14^{mKO}$ mice at the age of 10 weeks. $n = 5–7$ in each group. (C) Average four-paw grip strength of 10-week-old $Fn14^{fl/fl}$ and $Fn14^{mKO}$ mice. $n = 5–7$ in each group. (D) Average four-paw grip strength per gram of body weight of 10-week-old $Fn14^{fl/fl}$ and $Fn14^{mKO}$ mice. $n = 5–7$ in each group. Quantification of (E) oxygen consumption rate (VO2), (F) carbon dioxide production rate (VCO2), (G) respiratory exchange rate (RER; VCO2/VO2), (H) whole-body energy expenditure (Heat) (I) food and water intake over 24 h cycle of $Fn14^{fl/fl}$ and $Fn14^{mKO}$ mice. $n = 5–7$ in each group. After acclimatization, mice were run on a treadmill with a 10% slope and increasing speed to exhaustion. Maximum running time, speed, distance, work, and power were calculated based on individual performance. (J) Running time; (K) Speed; (L) Distance; (M) Work. $n = 7–12$ in each group. Quantification of normalized (N) peak tetanic force and (O) integration force over 30 sec. $n = 8–13$ in each group. Data are presented as mean ± SEM. $\#p \leq .05$, values significantly different from corresponding $Fn14^{fl/fl}$ mice by unpaired Student *t* test.

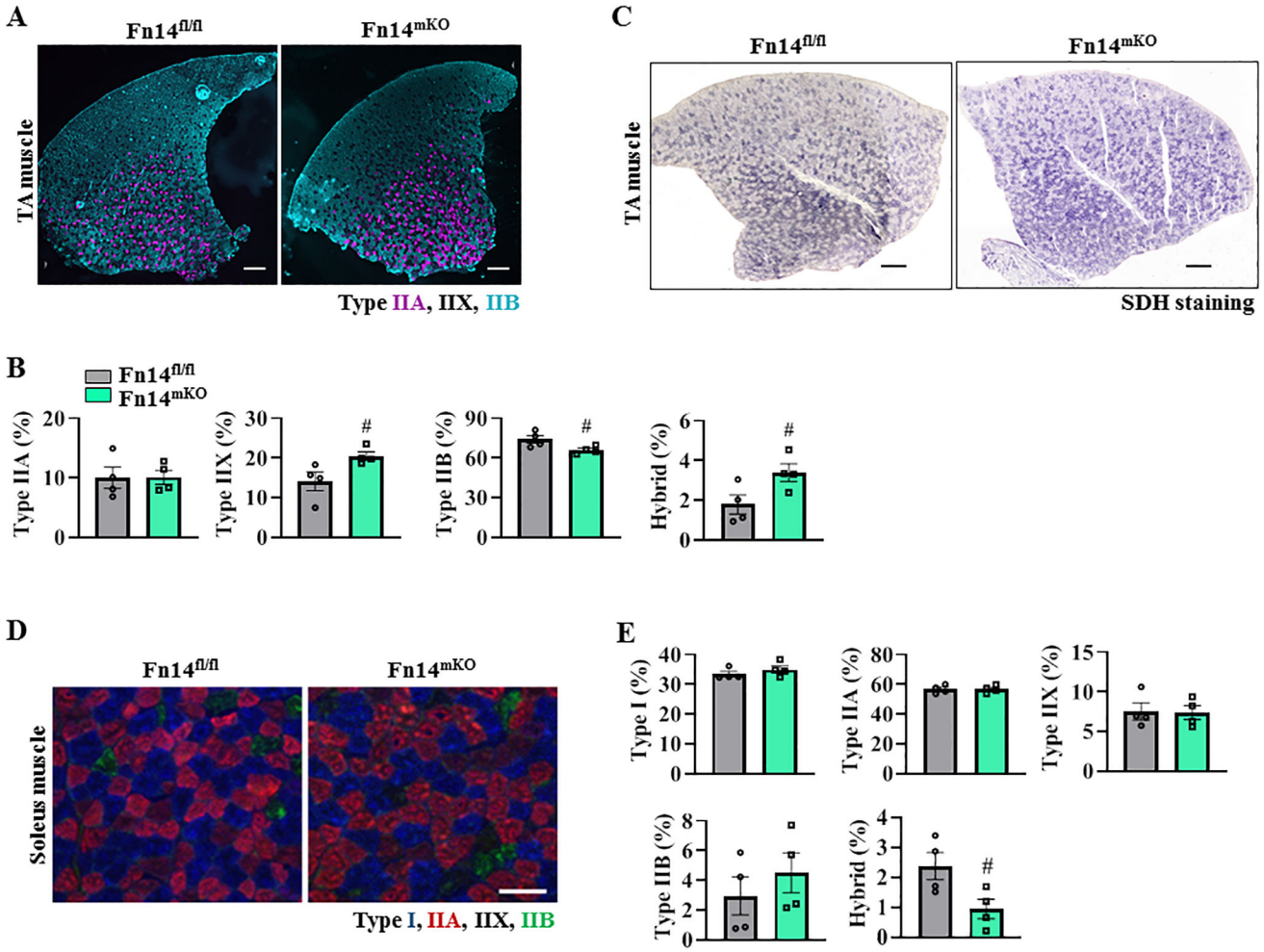


**FIGURE 2. Effect of muscle-specific deletion of Fn14 on the composition of slow and fast-type myofibers.**

(A) Representative images of transverse sections of TA muscle after staining for MyHC IIA and IIB protein. Scale bar: 300 μm. Quantification of percentage of (B) Type IIA, Type IIX, IIB, and intermediate fibers (Hybrid) in TA muscle of 10-week-old $Fn14^{fl/fl}$ and $Fn14^{mKO}$ mice. (C) Representative images of TA muscle sections after staining with SDH. Scale bar: 300 μm. (D) Representative images of transverse sections of soleus muscle after staining for MyHC I, IIA, and IIB protein. Scale bar: 50 μm. Quantification of percentage of (E) Type, I, IIA, IIX, IIB, and hybrid myofibers in soleus muscle of 10-week-old $Fn14^{fl/fl}$ and $Fn14^{mKO}$ mice. n = 4 in each group. Data are presented as mean ± SEM. #$p \leq .05$, values significantly different from corresponding $Fn14^{fl/fl}$ mice by unpaired Student *t* test.

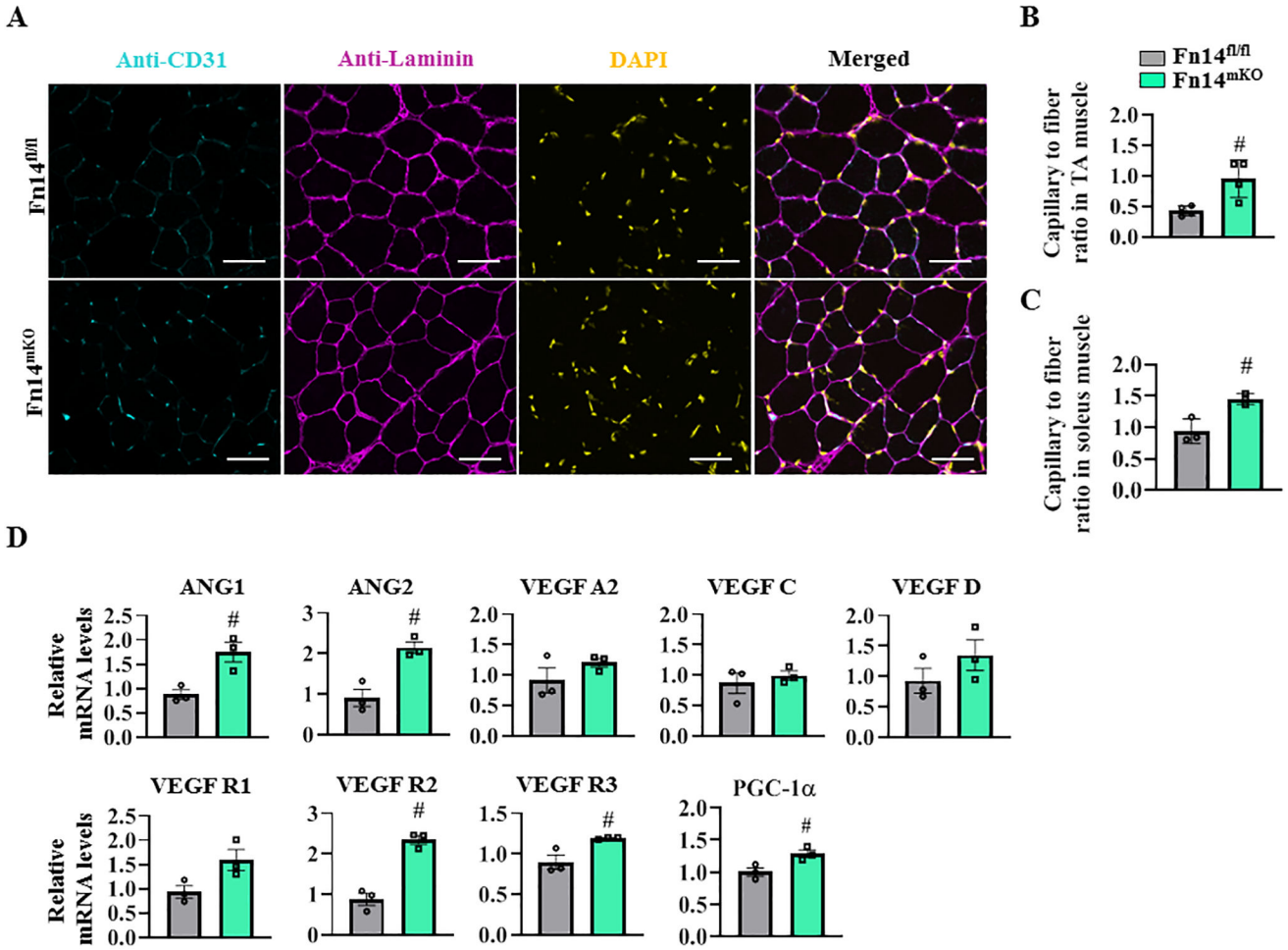


**FIGURE 3. Targeted deletion of Fn14 increases vascularization in skeletal muscle.**

(A) Transverse sections of TA muscle of $Fn14^{fl/fl}$ and $Fn14^{mKO}$ mice at the age of 10 weeks immunostained for CD31 (cyan), Laminin (magenta), and DAPI (yellow). Scale bar: 100 μm. (B) Quantification of CD31-positive capillaries per myofiber in TA muscle. (C) Quantification of CD31-positive capillaries per myofiber in soleus muscle of $Fn14^{fl/fl}$ and $Fn14^{mKO}$ mice. $n = 3–4$ in each group. (D) Relative mRNA levels of Ang1, Ang2, VEGF A2, VEGF C, VEGF D, VEGF R1, VEGF R2, VEGF R3, and PGC-1α in GA muscle of $Fn14^{fl/fl}$ and $Fn14^{mKO}$ mice assayed by performing qRT-PCR. $n = 3–4$ in each group. Data are presented as mean ± SEM. #$p \leq .05$, values significantly different from corresponding $Fn14^{fl/fl}$ mice by unpaired Student *t* test.

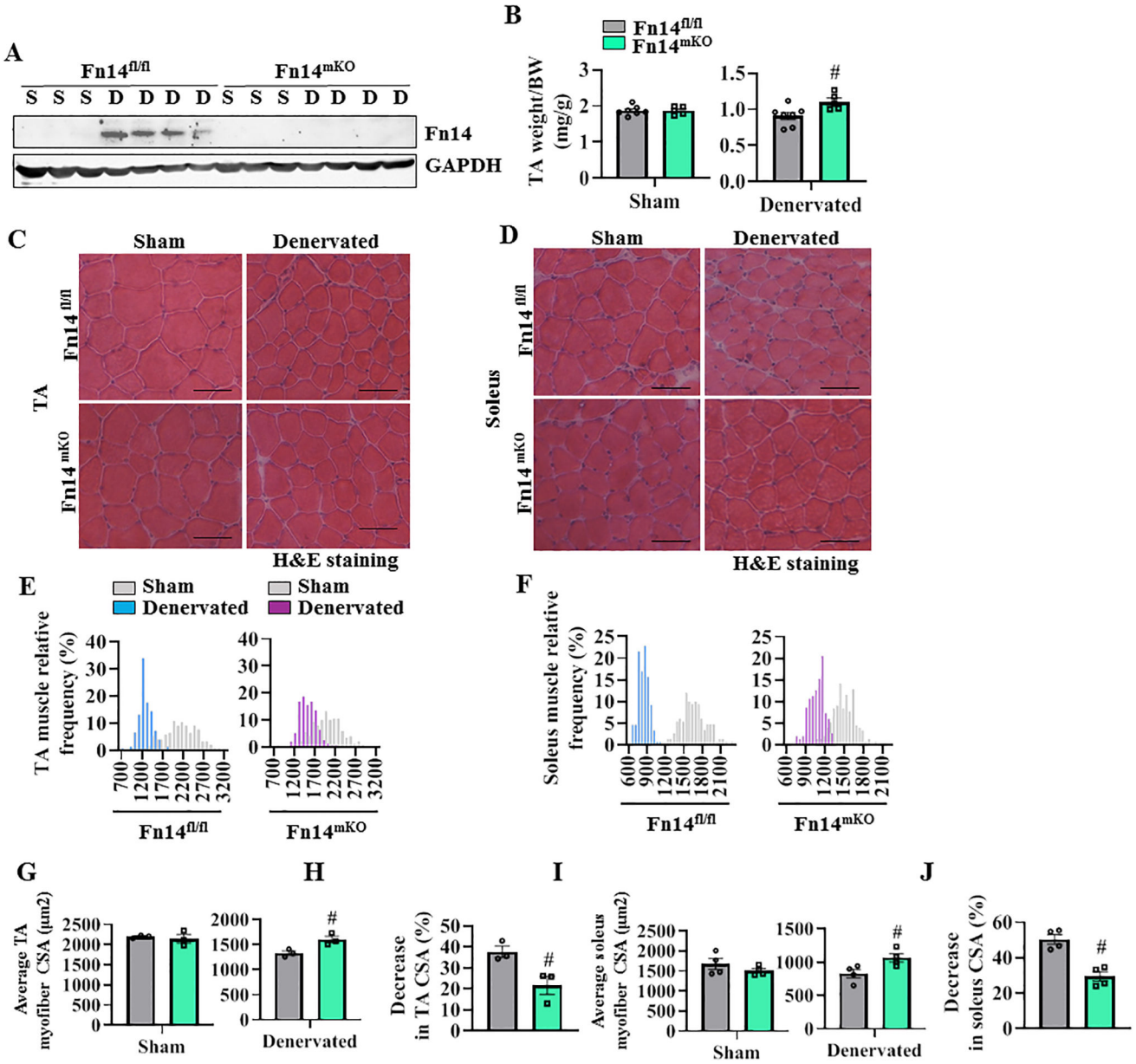


**FIGURE 4. Role of Fn14 in denervation-induced muscle atrophy.**

Littermate Fn14$^{fl/fl}$ and Fn14$^{mKO}$ mice at the age of 10 weeks were subjected to sham or denervation surgery for 14 days followed by isolation of hind limb muscles for biochemical and histological analysis. (A) Representative immunoblots showing levels of Fn14 and unrelated protein GAPDH in GA muscle of Fn14$^{fl/fl}$ and Fn14$^{mKO}$ mice. (B) Wet weight of TA muscle normalized by body weight in the sham-operated and denervated muscle of Fn14$^{fl/fl}$ and Fn14$^{mKO}$ mice. $n$ = 5–7 in each group. Representative photomicrographs of (C) TA and (D) soleus muscle sections after H&E staining. Scale bar: 50 μm. Relative frequency distribution of myofiber cross-section area (CSA) in sham-operated and denervated (E) TA and (F) soleus muscle of Fn14$^{fl/fl}$ and Fn14$^{mKO}$ mice. $n$ = 5–7 in each group. (G) Average myofiber CSA in sham-operated and contralateral denervated TA muscle of Fn14$^{fl/fl}$ and Fn14$^{mKO}$ mice. (H) Percent loss in average myofiber CSA in TA muscle of Fn14$^{fl/fl}$ and

$Fn14^{mKO}$ mice at day 14 post-denervation. $n = 3$ in each group. (I) Average myofiber CSA in sham-operated and contralateral denervated soleus muscle of $Fn14^{fl/fl}$ and $Fn14^{mKO}$ mice. (J) Percent loss in average CSA in soleus muscle of $Fn14^{fl/fl}$ and $Fn14^{mKO}$ mice at day 14 after denervation. $n = 4$ in each group. Data are presented as mean ± SEM. #$p \leq .05$, values significantly different from corresponding $Fn14^{fl/fl}$ mice by unpaired Student *t* test. D, denervated; S, sham.

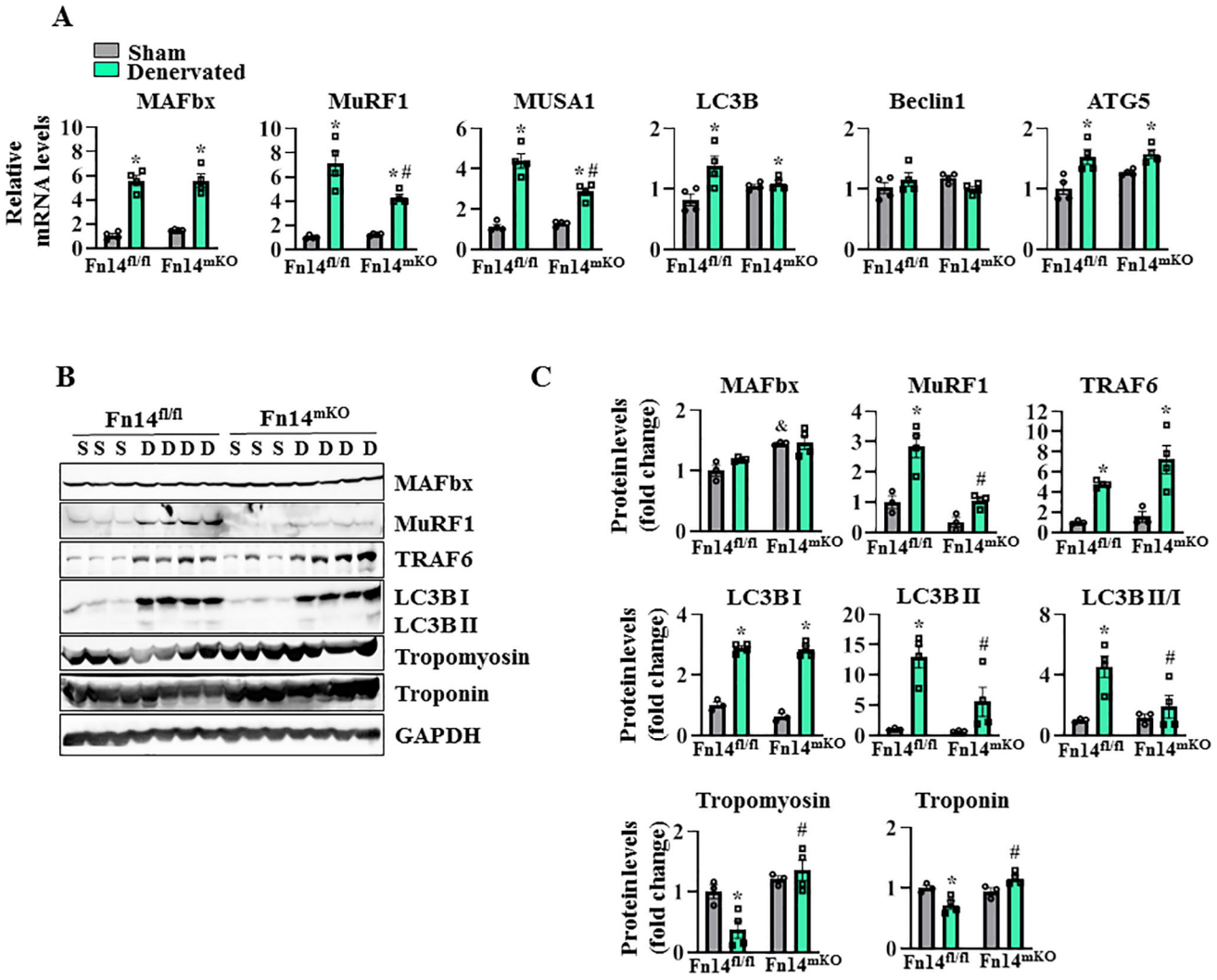


**FIGURE 5. Fn14 increases levels of components of UPS and autophagy in denervated muscle.**

Littermate Fn14$^{fl/fl}$ and Fn14$^{mKO}$ mice at the age of 10 weeks were subjected to sham or denervation surgery for 3 or 14 days followed by isolation of GA muscle for qRT-PCR and western blot analysis. (A) Relative mRNA levels of E3 ubiquitin ligases (MAFbx, MuRF1, MUSA1) and autophagy markers (LC3B, Beclin1, ATG5) in sham-operated and 3 days denervated muscle. $n = 4$ in each group. (B) Representative immunoblots, (C) densitometry analysis demonstrating levels of MAFbx, MuRF1, TRAF6, LC3B I, LC3B II, Tropomyosin, Troponin, and unrelated protein, GAPDH, in sham-operated and 14 days denervated muscle. $n = 3$–4 in each group. Data are presented as mean ± SEM and were analyzed by two-way ANOVA followed by Tukey's multiple comparison test. *$p \leq .05$, values significantly different from sham-operated corresponding GA muscle. #$p \leq .05$, values significantly different from 3 or 14 days denervated GA muscle of Fn14$^{fl/fl}$ mice. &$p \leq .05$, values significantly different from sham-operated GA muscle of Fn14$^{fl/fl}$ mice. D, denervated; S, sham.

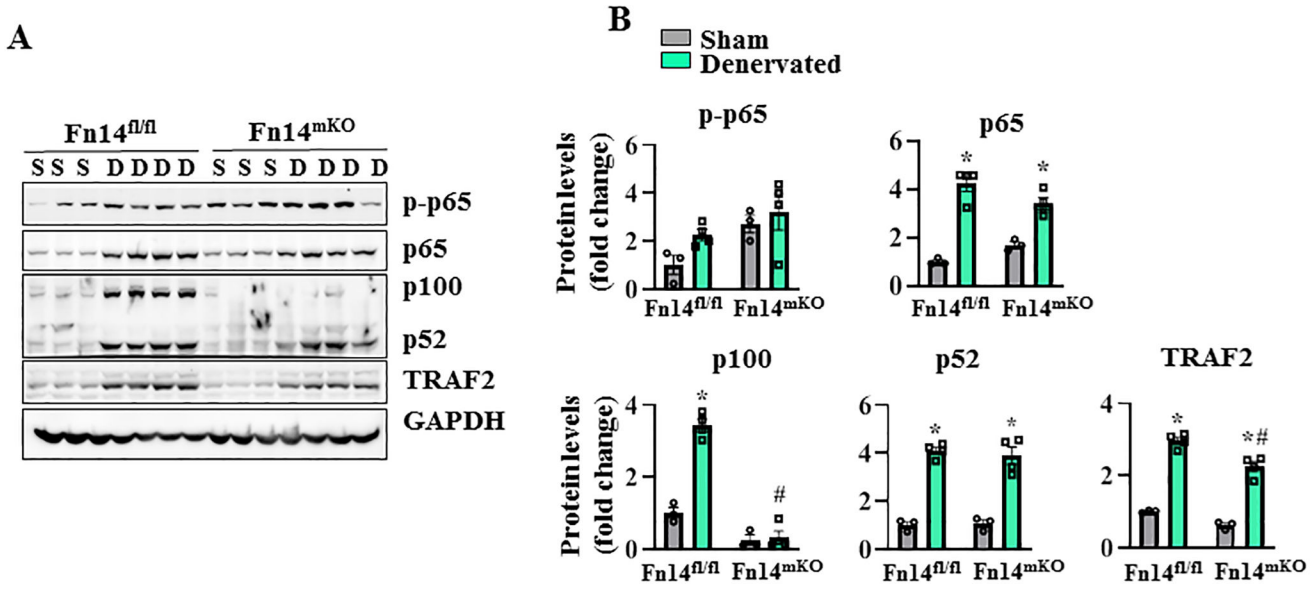


**FIGURE 6. Role of Fn14 in the activation of NF-κB signaling in denervated muscle.**

Littermate Fn14$^{fl/fl}$ and Fn14$^{mKO}$ mice at the age of 10 weeks were subjected to sham or denervation surgery for 14 days followed by isolation of GA muscle for western blot analysis. (A) Representative immunoblots (B) densitometry analysis demonstrating levels of phosphorylated p65 (p-p65), p65, p100, p52, TRAF2, and unrelated protein, GAPDH, in sham-operated and 14 days denervated muscle. $n = 3–4$ in each group. Data are presented as mean ± SEM and were analyzed by two-way ANOVA followed by Tukey's multiple comparison test. *$p \leq .05$, values significantly different from sham-operated corresponding GA muscle. #$p \leq .05$, values significantly different from 14 days denervated GA muscle of Fn14$^{fl/fl}$ mice. D, denervated; S, sham.

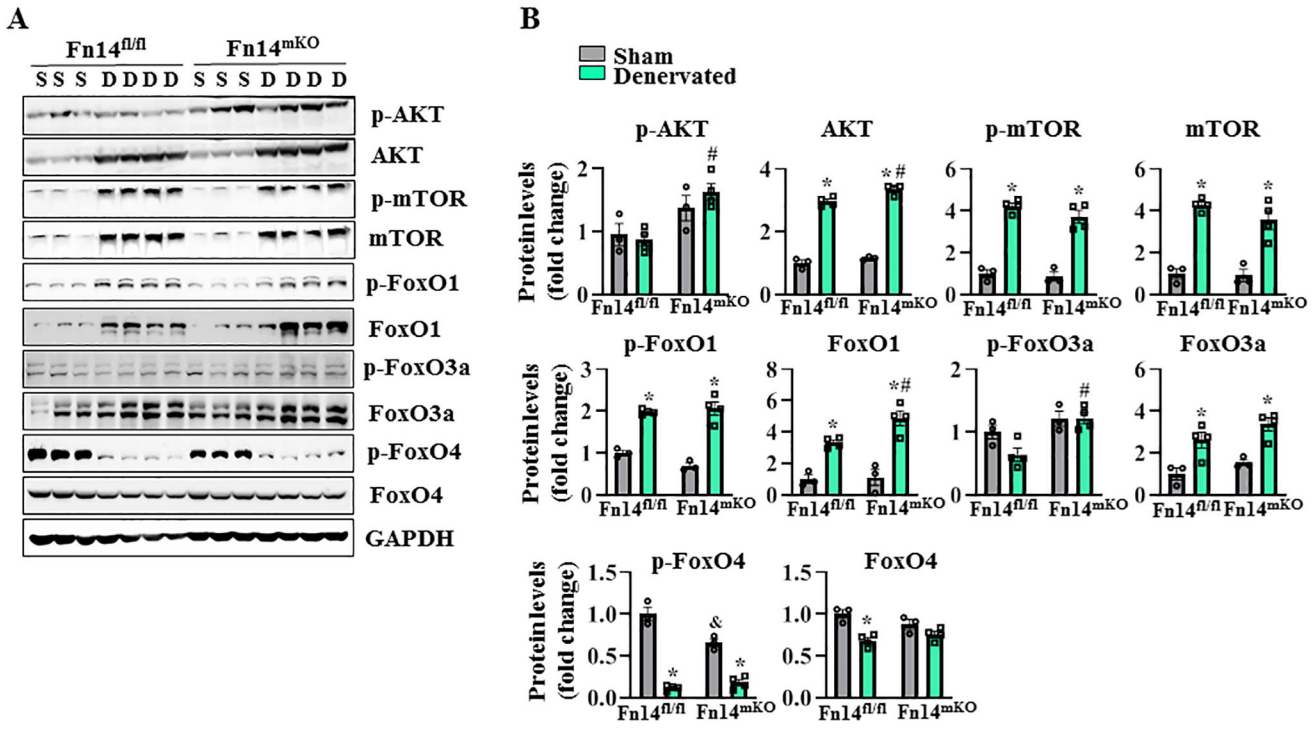


**FIGURE 7. Role of Fn14 in the regulation of Akt/FOXO phosphorylation.**

Littermate 10-week-old $Fn14^{fl/fl}$ and $Fn14^{mKO}$ mice were subjected to sham or denervation surgery for 14 days followed by isolation of GA muscle for western blot analysis. (A) Representative immunoblots and (B) densitometry analysis demonstrating levels of p-AKT, AKT, p-mTOR, mTOR, p-FoxO1, FoxO1, p-FoxO3a, FoxO3a, p-FoxO4, FoxO4 and unrelated protein, GAPDH in sham-operated and 14 days denervated muscle. $n = 3–4$ in each group. Data are presented as mean ± SEM and were analyzed by two-way ANOVA followed by Tukey's multiple comparison test. *$p \leq .05$, values significantly different from sham-operated corresponding GA muscle. #$p \leq .05$, values significantly different from 14 days denervated GA muscle of $Fn14^{fl/fl}$ mice. & $p \leq .05$, values significantly different from sham-operated GA muscle of $Fn14^{fl/fl}$ mice. D, denervated; S, sham.